

Optimal SSB Beam Planning and UAV Cell Selection for 5G Connectivity on Aerial Highways

Matteo Bernabè^{*†}, David López-Pérez[‡], Nicola Piovesan^{*}, Giovanni Geraci^{§¶}, and David Gesbert[†]

^{*}Huawei Technologies, France [†]EURECOM, France [‡]iTeam, Universitat Politècnica de València, Spain

[§]Telefónica Research, Spain [¶]Universitat Pompeu Fabra, Spain

Abstract— In this article, we introduce a method to optimize 5G massive multiple-input multiple-output (mMIMO) connectivity for unmanned aerial vehicles (UAVs) on aerial highways through strategic cell association. UAVs operating in 3D space encounter distinct channel conditions compared to traditional ground user equipment (gUE); under the typical line of sight (LoS) condition, UAVs perceive strong reference signal received power (RSRP) from multiple cells within the network, resulting in a large set of suitable serving cell candidates and in low signal-to-interference-plus-noise ratio (SINR) due to high interference levels. Additionally, a downside of aerial highways is to pack possibly many UAVs along a small portion of space which, when taking into account typical LoS propagation conditions, results in high channel correlation and severely limits spatial multiplexing capabilities. In this paper, we propose a solution to both problems based on the suitable selection of serving cells based on a new metric which differs from the classical terrestrial approaches based on maximum RSRP. We then introduce an algorithm for optimal planning of synchronization signal block (SSB) beams for this set of cells, ensuring maximum coverage and effective management of UAVs cell associations. Simulation results demonstrate that our approach significantly improves the rates of UAVs on aerial highways, up to four times in achievable data rates, without impacting ground user performance.

I. INTRODUCTION

Unmanned aerial vehicles (UAVs) have emerged as a key technology across multiple market sectors, including photography, infrastructure inspection and disaster management [1]–[3]. Only in recent years have UAVs become an integral part of the urban scenario as well [4]. Overall, urban air mobility (UAM), including future transportation, cargo drones, and other civil applications, is expected to play a disruptive role in future markets, with recent reports projecting its value to reach 5.1 billion U.S. dollars by 2028 [5]. However, the burgeoning interest in UAVs within urban scenarios raises critical challenges: *i*) development of regulation for secure management in urban skies, *ii*) supporting reliable connectivity in the sky enabling beyond visual line of sight (BVLoS) applications. In terms of regulation, industries and regulatory bodies are working towards creating a highway system for the sky, namely aerial highways (AHs); similar to traditional ground road scenarios, AHs —also often denoted as UAV

This research was supported by *a*) the Generalitat Valenciana, Spain, through the CIDEGENT PlaGenT, Grant CIDEXG/2022/17, Project iTENTE, *b*) the action CNS2023-144333, financed by MCIN/AEI/10.13039/501100011033 and the European Union “NextGenerationEU”/PRTR, *c*) the Spanish State Research Agency through grants PID2021-123999OB-I00, CEX2021-001195-M, and CNS2023-145384, *d*) the UPF-Fractus Chair on Tech Transfer and 6G, and *e*) the Spanish Ministry of Economic Affairs and Digital Transformation.

corridors— are defined trajectories that UAVs must follow while pursuing their tasks [6], [7].

In recent years, studies identified in cellular networks the key technologies to enable BVLoS services [8]–[12]. Nevertheless, the optimal integration of cellular-connected UAVs in terrestrial networks remains a challenge, especially when considering AHs. Few pioneering works in the literature addressed this problem. In the context of AH supported by 4G networks, authors in [13] considered a set of uptilted sectors to serve the AH while providing, under specific assumptions, an analytical framework for outage probability. Similarly, authors in [14] deployed a new set of uptilted antennas while proposing a solution to mitigate the generated interference to the ground. In our previous work [15], we introduced an ADAM-based solution to optimize the vertical tilt of 4G base stations for user equipment (UE) on the ground and along AHs without the need for new infrastructure. Driven by similar motivations, authors in [16] and in [17] respectively proposed quantization theory- and Bayesian optimization-based approaches to design cell antenna tilt and transmit power and optimally cover both ground user equipments (gUEs) and UAVs within AHs.

In 5G, massive multiple-input multiple-output (mMIMO) offers a paradigm shift and is capable of enhancing UAVs communications too [18]–[20]. Previous studies that showed significant advantages of optimizing serving cells in mMIMO ultra dense networks (UDNs) [21], [22], suggest that similar principles benefit UAV in urban macro (UMa) scenarios. Indeed, the typical line of sight (LoS) for UAVs creates similar cell association dynamics as in UDNs, therefore controlling cell association along the AH become crucial for improving UAVs connectivity. Unlike the real-time centralized schedulers proposed in previous work, new solutions are needed to tackle the problem at the radio access network planning stage.

In this work we demonstrate how leveraging the prior knowledge of the AH trajectory to plan and control the transmitted synchronization signal block (SSB) beams, and in turn the UAVs cell association processes, allows to efficiently optimize connectivity on AHs. Specifically, we propose a new metric to optimally define the set of cells aimed to serve UAVs, by jointly considering multiplexing capability, average channel gain, and interference of each cell. Furthermore, we propose an elite genetic algorithm (eGA) to optimally select SSB beams and their transmit power within the set of identified cells, thereby ensuring desired cell association.¹

¹Extensions of this work can be found in [23].

II. SYSTEM MODEL

We focus on a downlink, interference-limited scenario, with models as defined by the 3rd Generation Partnership Project (3GPP).

Network deployment: We consider a cellular network operating in a sub-6 GHz band (FR1), with carrier frequency f_c and bandwidth B_0 . The network layout consists of 19 sites, organized in a 2-tier hexagonal grid, with an inter-site distance d_{ISD} . Each site is composed of three sectors², each covering 120°. The complete set of sectors is denoted by \mathcal{B} , with N_{BS} denoting its cardinality. Full frequency reuse is applied in all sectors. Each sector contains a uniform planar array (UPA) antenna panel located at a height h_{BS} , consisting of M single vertically polarized antenna elements, arranged in M_h horizontal and M_v vertical rows. The total number of physical resource blocks (PRBs) available is N_{PRB} , each with a bandwidth of B_{PRB} .

Terrestrial users: Assuming a fully loaded scenario, we consider a total of N_g gUEs randomly distributed in all cells. Additionally, to capture the dynamic nature of the network, the positions of gUEs randomly vary over time.

Aerial users: An AH \mathbf{r}_{AH} , spanning a total length of L_{AH} , is positioned over multiple cell centres and edges of our scenario at an altitude of h_{AH} . For simplicity, we consider that the AH is divided into N_{seg} consecutive segments. Over the aforementioned AH, a total number of N_a UAVs are evenly spaced with constant inter-UAV distance (IUD) d_{IUD} ; all the defined UAVs move along the AH while maintaining same d_{IUD} . To maintain continuous aerial traffic, note that when one UAV exits, another enters the AH.

We denote by \mathcal{G} the set of all gUEs, by \mathcal{A} the set of UAVs and by \mathcal{U} the set of all UEs, such that $\mathcal{U} = \mathcal{G} \cup \mathcal{A}$.

A. Channel Model

We consider the 3GPP statistical channel models defined in [24] and [25].

Large-scale fading: For each UE $u \in \mathcal{U}$ and sector $b \in \mathcal{B}$, the large-scale channel between them is obtained from the LoS probability P_{LoS} , path loss gain $\rho_{u,b}$, antenna element gain $g_{u,b}$, and shadow fading gain $\tau_{u,b}$. Note that the shadow fading gain is modelled as spatially correlated as per the 3GPP recommendations. Using the 3GPP models, we can then define the large-scale gain $\beta_{u,s}$ as follows:

$$\beta_{u,b} = \rho_{u,b} \tau_{u,b} g_{u,b}. \quad (1)$$

Small-scale fading: To model the small-scale fading, the downlink complex channel vector between each UE u and each antenna element m of each sector b is defined as follows:

$$\mathbf{h}_{u,b}^{\text{dl}} = \sqrt{\frac{K}{1+K}} \mathbf{h}_{u,b}^{\text{LOS}} + \sqrt{\frac{1}{1+K}} \mathbf{h}_{u,b}^{\text{NLOS}}, \quad (2)$$

where K is the so-called Rician Factor [24], [25]. The LoS component of the channel follows the plane-wave approximation [26], thus representing the phase shift of the plane wave

with respect to each antenna element of the antenna panel. It is computed as follows:

$$\mathbf{h}_{u,b}^{\text{LOS}} = e^{-j \frac{2\pi}{\lambda_c} d_{u,b}^{3\text{D}}} e^{j \frac{2\pi}{\lambda_c} \mathbf{k}_{u,b}^T(\phi_{u,b}, \theta_{u,b}) \mathbf{U}_b} \quad (3)$$

with

$$\mathbf{k}_{u,b} \in \mathbb{R}^{3 \times 1}, \quad \mathbf{U}_b \in \mathbb{R}^{3 \times M}, \quad (4)$$

where λ_c is the frequency wavelength associated with the carrier frequency f_c , $d_{u,b}^{3\text{D}}$ is the 3D distance between UE u and the antenna panel centre of sector b , $\mathbf{k}_{u,b}^T(\phi_{u,b}, \theta_{u,b})$ is the wave vector representing the plane wave variations in the 3D space, and \mathbf{U}_b is the matrix containing the Cartesian coordinates of each antenna element w.r.t. the antenna panel centre. The non-line of sight (NLoS) component of the channel is modeled as a Rayleigh fading complex channel as follows:

$$\mathbf{h}_{u,b}^{\text{NLOS}} \sim \text{CN}(\mathbf{0}, \mathbf{I}_M). \quad (5)$$

B. Cell Association and Precoding

One of the physical layer features introduced in 5G new radio (NR) is the beamforming capability during the initial cell discovery phase via SSB beams, which allows sectors to cover different sections of their designated areas efficiently. Specifically, in a network operating in the sub-6 GHz band, referred to as frequency range 1 (FR1), each sector b can transmit up to 8 SSB beams [27]. These beams are multiplexed sequentially in time, following a sweep pattern associated with their sweep index i_s^{SSB} .

SSB beams codebook: At each sector b , each SSB beam s is represented by a complex codeword $\mathbf{w}_{s,b}^{\text{SSB}}$ and is selected from a predetermined SSB codebook \mathbf{W}^{SSB} . We assume each antenna element of the planar array to be connected to a distinct transceiver. To accommodate beams with varying beamwidths and beamforming gains, we employ a switching pattern that sequentially deactivates antenna columns from the rightmost to the leftmost on the panel. For each configuration, we generate an intermediate SSB codebook $\mathbf{W}_i^{\text{SSB}}$ through a two dimensional discrete Fourier transform (2D-DFT), and subsequently aggregate these into the general SSB codebook \mathbf{W}^{SSB} , which consists of N_{CB} codewords.

Cell association: To identify its serving cell, each UE u measures the reference signal received power (RSRP) from each cell b and each SSB beam s . The measured RSRP is defined as follows:

$$\text{rsrp}_{u,s,b}^{\text{SSB}} = \beta_{u,b} \left| \mathbf{h}_{u,b}^{\text{dl}} \mathbf{w}_{s,b}^{\text{SSB}} \right|^2 p_{s,b}^{\text{SSB}} x_{s,b}, \quad (6)$$

where $x_{s,b} \in \mathbf{X}$ is a binary variable, equal to one if beam s is deployed at cell b , and zero otherwise. The transmit power allocated by sector b to beam s , denoted by $p_{s,b}^{\text{SSB}}$, is an element of the matrix \mathbf{P} . The matrices \mathbf{X} and \mathbf{P} together provide a network-wide representation of the deployed beams and their transmit powers. For each UE u , the serving cell \hat{b}_u and beam \hat{s}_u are defined as those that maximize the measured RSRP (6).

²In the rest of the paper, the terms ‘‘sector’’ and ‘‘cell’’ are used as synonyms.

$$\gamma_u = \frac{\beta_{u,\hat{b}_u} \left| \mathbf{h}_{u,\hat{b}_u}^{\text{dl}} \mathbf{w}_{u,\hat{b}_u}^{\text{dl}} \right|^2 p_{u,\hat{b}_u}^{\text{dl}}}{\beta_{u,\hat{b}_u} \sum_{p \in \mathcal{U}_{\hat{b}_u} \setminus u} \left(1 - \delta \left(\mathbf{w}_{u,\hat{b}_u}^{\text{dl}}, \mathbf{w}_{p,\hat{b}_u}^{\text{dl}} \right) \right) \left| \mathbf{h}_{u,\hat{b}_u}^{\text{dl}} \mathbf{w}_{p,\hat{b}_u}^{\text{dl}} \right|^2 p_{p,\hat{b}_u}^{\text{dl}} + \sum_{b \in \mathcal{B} \setminus \hat{b}_u} \beta_{u,b} \sum_{\mathbf{w}_{i,b}^{\text{dl}} \in \mathbf{W}_b^{\text{dl}}} \frac{1}{N_{\mathbf{w}_{i,b}^{\text{dl}}}} \left| \mathbf{h}_{u,b}^{\text{dl}} \mathbf{w}_{i,b}^{\text{dl}} \right|^2 p_{i,b}^{\text{dl}} + \frac{N_{\text{PRB}} B_{\text{PRB}}}{N_{\mathbf{w}_{u,\hat{b}_u}^{\text{dl}}}} N_0} \quad (8)$$

For each UE u , we define the coverage signal-to-interference-plus-noise ratio (SINR) γ_u^{ssb} as follows:

$$\gamma_u^{\text{ssb}} = \frac{\text{rsrp}_{u,\hat{s}_u,\hat{b}_u}^{\text{ssb}}}{\sum_{b=1, b \neq \hat{b}}^{N_{\text{BS}}} \sum_{s=1}^{N_{\text{ssb}}} \text{rsrp}_{u,s,b}^{\text{ssb}} \delta(i_{\hat{s}_u}^{\text{ssb}}, i_s^{\text{ssb}}) x_{s,b} + N_u}, \quad (7)$$

where $\delta(i_{\hat{s}_u}^{\text{ssb}}, i_s^{\text{ssb}})$ is defined as a binary function that takes a value of one if, and only if, $i_{\hat{s}_u}^{\text{ssb}} = i_s^{\text{ssb}}$.

C. SINR and Achievable Data Rate

Data transmission phase: To leverage the beamforming and multiplexing capabilities of NR mMIMO systems, we consider a Type I channel state information (CSI)-based operational approach [27], [28]. In this NR network setup, each UE reports a set of measurement indices to its serving cell. Based on these, the sector chooses a specific codeword from a codebook, defined by 2D-DFT and considering all transceiver active, to precode the UE's data. Specifically, the sector b selects, for each UE u , the downlink precoding vector $\mathbf{w}_{u,\hat{b}_u}^{\text{dl}}$ as follows:

$$\mathbf{w}_{u,\hat{b}_u}^{\text{dl}} = \underset{\mathbf{w} \in \mathbf{W}^{CB}}{\text{argmax}} \left\{ \beta_{u,b} \left| \mathbf{h}_{u,\hat{b}_u}^{\text{dl}} \mathbf{w} \right|^2 \right\}. \quad (9)$$

SINR and achievable rate: The resulting SINR at UE u is computed according to (8). In this framework, \mathcal{U}_b represents the subset of UEs associated with cell b , and $\mathbf{h}_{u,b}^{\text{dl}}$, $\mathbf{w}_{u,b}^{\text{dl}}$, and $p_{u,b}^{\text{dl}}$ are the downlink complex channel vector, the precoding codeword, and the associated transmit power of UE u with respect to cell b , respectively. Without loss of generality, we assume equal transmit power allocation for all UEs. The achievable data rate for each UE can be then computed as follows:

$$R_u = \frac{N_{\text{PRB}}^{\text{tot}} B_{\text{PRB}}}{N_{\mathbf{w}_{u,\hat{b}_u}^{\text{dl}}}} \log_2(1 + \gamma_u), \quad (10)$$

where $N_{\mathbf{w}_{u,\hat{b}_u}^{\text{dl}}}$ is the number of UE associated with the same precoding codeword and N_0 is the thermal noise power spectral density.

III. CELL SELECTION AND SSB BEAM PLANNING

The performance of mMIMO networks is affected by the complex interplay of many system parameters, making its modelling and large-scale optimization a challenging task. To tackle this problem, we propose an efficient solution to maximize UAVs data rates along AH by optimally controlling UAVs cell association along the AH. To this end, we first introduce a new metric to identify the optimal serving cell for each segment of an AH. Then, we develop an eGA algorithm to optimally select SSB beams and their transmit power from a fixed codebook, ensuring optimal coverage from those cells.

A. Aerial Highway Segment-to-Cell Association Metric

In traditional cellular networks, serving cells are typically selected based on metrics such as RSRP. While this metric may be suitable for gUEs, it often falls short for UAVs closely packed along the AH, where the high channel correlation, driven by dominant LoS conditions [29], can severely affect network performance. To optimally determine the cells designated to serve UAVs along the pre-defined AH, we now introduce a novel metric that captures the multiplexing capability, average channel quality gain, and interference.

Aerial highway Segmentation: We begin by discretizing the AH \mathbf{r}_{AH} into N_r equidistant points separated by distance d_r . Utilizing simulations and/or measurements gathered during exploratory phases, one may determine the expected channel vector $\tilde{\mathbf{h}}_{r,b}$ for each point r relative to each cell b as follows,

$$\tilde{\mathbf{h}}_{r,b} = \mathbb{E}_{\tau, \mathbf{h}^{\text{dl}}} \left[\rho_{r,b} \tau_{r,b} g_{r,b} \mathbf{h}_{r,b}^{\text{dl}} \right]. \quad (11)$$

We utilize these vectors to construct the average complex channel matrix $\tilde{\mathbf{H}}_{r,m}^b \in \mathbb{C}^{N_r \times M}$ between the AH and each cell b . Subsequently, we introduce the concept of a segment \mathbf{z} , which represents a contiguous subset of N_s points within said AH \mathbf{r}_{AH} . Then, from matrix $\tilde{\mathbf{H}}_{r,m}^b$, we define two sub-matrices $\tilde{\mathbf{H}}_{z,m}^b$ and $\tilde{\mathbf{H}}_{r-z,m}^b$, respectively denoting the complex channel vectors of segment \mathbf{z} and of the remaining AH discrete points.

Cell association metric: We define our proposed mMIMO-Aerial-Metric-Association (MAMA) metric as follows:

$$\begin{aligned} \chi_{\mathbf{z}}^b \left(\tilde{\mathbf{H}}_{z,m}^b, \tilde{\mathbf{H}}_{r-z,m}^b \right) &= \\ &= c_{\mathbf{z}}^b \left(\tilde{\mathbf{H}}_{z,m}^b \right) \log_2 \left(1 + \frac{P_{\mathbf{z}}^b \left(\tilde{\mathbf{H}}_{z,m}^b \right)}{F_{\mathbf{z}}^b \left(\tilde{\mathbf{H}}_{z,m}^b, \tilde{\mathbf{H}}_{r-z,m}^b \right) + N_0} \right). \end{aligned} \quad (12)$$

The metric in (12) is composed of three components, designed to account for different channel characteristics, specifically:

- $P_{\mathbf{z}}^b$ is the expected average channel gain on segment \mathbf{z} when served by cell b . It is computed as follows,

$$P_{\mathbf{z}}^b \left(\tilde{\mathbf{H}}_{z,m}^b \right) = \frac{1}{N_z} \sum_z \frac{1}{M} \sum_{m=0}^{M-1} |h_{z,m}^b|^2, \quad (13)$$

and it encapsulates traditional metrics like RSRP.

- $c_{\mathbf{z}}^b$ is the inverse of the condition number of matrix $\tilde{\mathbf{H}}_{z,m}^b$. It is computed as follows:

$$c_{\mathbf{z}}^b \left(\tilde{\mathbf{H}}_{z,m}^b \right) = \frac{\lambda_{\mathbf{z}}^{b(M-1)} \left(\tilde{\mathbf{H}}_{z,m}^b \right)}{\lambda_{\mathbf{z}}^{b(0)} \left(\tilde{\mathbf{H}}_{z,m}^b \right)}, \quad (14)$$

where $\lambda_{\mathbf{z}}^{b(M-1)}$ and $\lambda_{\mathbf{z}}^{b(0)}$ denote, respectively, the lowest and the highest singular values computed using single

value decomposition (SVD). This ratio provides insight into the spread of singular values, reflecting diversity in angle of arrivals (AoAs)/angle of departures (AoDs) and assessing multiplexing capabilities of cell b concerning segment \mathbf{z} .

- $F_{\mathbf{z}}^b$ represents the squared Frobenius norm of the cross-channel correlation. It is computed as follows:

$$F_{\mathbf{z}}^b \left(\tilde{\mathbf{H}}_{z,m}^b, \tilde{\mathbf{H}}_{r-z,m}^b \right) = \sum_i^{N_r - N_z} \sum_z^{N_z} \left| \sum_m \tilde{h}_{i,m}^b \tilde{h}_{m,z}^{b*} \right|^2. \quad (15)$$

This component provides information about the correlation between the considered segment and the remaining points of the AH, thereby assessing the interference level introduced to other portions of the AH when cell b serves segment \mathbf{z} .

Having divided the AH into N_{seg} segments, and having defined a cell association metric, one can then compute the serving cell $\hat{b}_{\mathbf{z}}$ for each segment \mathbf{z} as follows:

$$\hat{b}_{\mathbf{z}} = \underset{b \in \mathcal{B}}{\text{argmax}} \left\{ \chi_{\mathbf{z}}^b \left(\tilde{\mathbf{H}}_{z,m}^b, \tilde{\mathbf{H}}_{r-z,m}^b \right) \right\}. \quad (16)$$

In the sequel, we denote by $\hat{\mathbf{b}}^{(\text{AH})}$ the set of serving cells for all segments.

B. SSB Beam and Power Selection Algorithm

Given our proposed serving cell selection metric, we now propose an algorithm to optimally select the set of SSB beams and their transmit power from the codebook \mathbf{W}^{ssb} . These SSB beams are then to be transmitted at each identified serving cell to guarantee the desired association of UAVs that are flying in segment \mathbf{z} . In other words, our objective is to find the optimal binary entries of \mathbf{X} and \mathbf{P} , governing the selected SSBs beams and their respective power, that maximize a specific objective function—later defined in (18)—and, consequently, maximizing the minimum SINR (7) across the AH.

Before describing our solver, we find it convenient to define matrices \mathbf{X}^{bl} and \mathbf{P}^{bl} , representing the network configuration in a traditional scenario with only gUEs. We also list the constraints that our algorithm obeys:

- Only serving cells in $\hat{\mathbf{b}}^{(\text{AH})}$ are permitted to modify their SSB beam configuration. Conversely, cells not in this set must adhere to the configurations described by \mathbf{X}^{bl} and \mathbf{P}^{bl} .
- Cells in $\hat{\mathbf{b}}^{(\text{AH})}$ are allowed to modify only one SSB from the configuration in \mathbf{X}^{bl} and \mathbf{P}^{bl} , thus minimizing large deviations from the well optimized traditional scenario.
- The power associated with each modified SSB beam is limited to $p_{\text{max}}^{\text{ssb}}$.
- The serving cell for each point r of each segment \mathbf{z} must be $\hat{b}_{\mathbf{z}}$.

To solve this problem, we design an algorithm based on eGA [30]–[32], known for its efficiency in solving non-convex non-linear mixed-integer problems.

Preliminaries on eGA: In eGA, a solution emerges from a population of N_{pop} individuals, which iteratively transforms according to a objective (fitness) $\text{Obj}^{\text{eGA}}(\cdot)$. At each iteration, the population evolves following these steps:

- *Selection*, where individuals are ranked according to their fitness function, and N_p best individuals are selected as parents for generating the offspring, i.e., next population individuals.
- *Crossover*, where with a certain probability P_{cross} elements \mathbf{y}_q of each pair of parents are randomly exchanged. We refer to these newly obtained vectors as offspring.
- *Mutation*, where elements of the offspring vectors are randomly changed with probability P_{mut} .
- *Elastic Mechanism*, where the top N_e individuals are directly passed to the next population without crossover and mutation mechanisms.

For each iteration, the optimal solution is selected as the

Algorithm 1: elite Genetic Algorithm Beam Selection

Result: \mathbf{y}^{best}

```

1  $\mathbf{y}^{(p)} \leftarrow \text{init\_random\_population}(N_{\text{pop}}, N_{\text{CB}}, p_{\text{max}}^{\text{ssb}});$ 
2  $\mathbf{f} \leftarrow \text{init\_zeros}(N_{\text{pop}});$ 
3 for  $i \in [0, N_{\text{eGA}}^{\text{iter}} - 1]$  do
4   for  $q \in [0, N_{\text{pop}} - 1]$  do
5      $\mathbf{f}[q] \leftarrow \text{Obj}^{\text{eGA}}(\mathbf{y}^{(q)});$ 
6   end
7    $\text{sort\_population}(\mathbf{f});$ 
8    $\mathbf{y}^{\text{best}} \leftarrow \mathbf{y}^{(0)};$ 
9    $\text{par}_e \leftarrow [\mathbf{y}^{(0)}, \mathbf{y}^{(N_e)}];$ 
10   $\text{par}_q \leftarrow [\mathbf{y}^{(0)}, \mathbf{y}^{(N_p)}];$ 
11  for  $q \in N_{\text{cross}}$  do
12     $\mathbf{y}^{(i)}, \mathbf{y}^{(j)} \leftarrow \text{randomUniform\_selPair}(\text{par}_q);$ 
13    for  $k \in [0, 2n_s - 1]$  do
14      if  $\text{random}() \leq P_{\text{cross}}$  then
15         $\mathbf{y}^{(i)}[k], \mathbf{y}^{(j)}[k] \leftarrow \mathbf{y}^{(j)}[k], \mathbf{y}^{(i)}[k];$ 
16      end
17    end
18  end
19  for  $q \in [0, [N_{\text{pop}} - 1]]$  do
20    for  $k \in [0, n_s - 1]$  do
21      if  $\text{random}() \leq P_{\text{mut}}$  then
22         $\mathbf{y}^{(q)}[k] \leftarrow \text{randInt}(0, N_{\text{CB}} - 1);$ 
23      end
24    end
25    for  $k \in [n_s, 2n_s - 1]$  do
26      if  $\text{random}() \leq P_{\text{mut}}$  then
27         $\mathbf{y}^{(q)}[k] \leftarrow \text{rand}(0, p_{\text{max}}^{\text{ssb}});$ 
28      end
29    end
30  end
31   $e \leftarrow 0;$ 
32  for  $q \in [N_{\text{pop}} - N_e, N_{\text{pop}} - 1]$  do
33     $\mathbf{y}^{(q)} \leftarrow \text{par}_e[e];$ 
34     $e \leftarrow e + 1;$ 
35  end
36   $\text{EarlyStopping\_Check}(i, N_{\text{eGA}}^{\text{stop}});$ 
37 end
```

individual with the best fitness value. The algorithm progresses through these steps until it either reaches the designated number of generations, N_{eGA}^{Iter} , or the optimal solution remains unchanged over a specific number of generations N_{eGA}^{stop} , therefore enabling an early stopping mechanism.

Proposed eGA beam selection algorithm: For our problem, each individual q of the population represents a possible solution and is defined by a vector as follows,

$$\begin{aligned} \mathbf{y}_q &= \left[\mathbf{s}_{\hat{b}_z} \mid \mathbf{P}_{\hat{b}_z}^{\text{ssb}} \right] = \\ &= \left[s_{b_0}, \dots, s_{b_z}, \dots, s_{b_{n_s}} \mid p_{b_0}^{\text{ssb}}, \dots, p_{b_z}^{\text{ssb}}, \dots, p_{b_{n_s}}^{\text{ssb}} \right], \end{aligned} \quad (17)$$

where $s_{b_z} \in [0, N_{\text{CB}}]$ represents the codeword index selected at cell b_z from a codebook containing N_{CB} entries, and $p_{b_z}^{\text{ssb}}$ represents its transmit power. The matrices \mathbf{X}_q and \mathbf{P}_q are then computed based on the above vector values. To evaluate the performance of each individual q , we define the objective (fitness) function as

$$\text{Obj}^{eGA}(\mathbf{y}_q) \doteq \min \left\{ \gamma_z^{\text{ssb}} \mid z \in \mathbf{z}, \hat{b}_z = \hat{b}_z^{(\text{AH})}, \mathbf{X}_q, \mathbf{P}_q \right\}. \quad (18)$$

The objective function in (18) represents the minimum SINR across all the AH to be maximized. In particular, γ_z^{ssb} is the SSB SINR for point z , as defined in (7), conditioned on $\hat{b}_z^{(\text{AH})}$ being the serving cell for point z and \mathbf{X}_q and \mathbf{P}_q being the selected SSBs beams and their transmit powers, respectively.

Algorithm 1 illustrates the detailed steps.

IV. SIMULATION RESULTS

In this section, we evaluate the performance of our proposed SSB beam planning and UAV cell selection. Utilizing the models presented in Section II, we focus on UMa environments where each sector employs an 8×4 UPA panel operating at 3.5 GHz. The study considers a 1250 m AH located 100 m above the ground and crossing multiple cell edges. Then, ensuring 100 m inter-UAVs distance d_{TUD} [33], 12 UAVs are evenly spaced along this highway, and four gUEs are randomly deployed within each cell.

Performance benchmark: We compare the results obtained by our solution (“Opt”) to those of a baseline configuration where the terrestrial network is optimized solely for serving gUEs (“Baseline”). The baseline configuration positions all SSB beams at each cell with a tilt of 105° , covering the azimuth plane as recommended by the 3GPP [24]. The matrices \mathbf{X}^{bl} and \mathbf{P}^{bl} are then computed accordingly.

Algorithm parameters and convergence: In Algorithm 1, we choose a population size $N_{\text{pop}} = 100$, a number of parents $N_p = 75$, a number of elites $N_e = 20$, and we set the probabilities of crossover and mutation to $P_{\text{cross}} = 0.2$ and $P_{\text{mut}} = 0.75$, respectively. We set the maximum number of iterations to $N_{eGA}^{\text{Iter}} = 15000$ and the early stopping criterion to $N_{eGA}^{\text{stop}} = 1000$ iterations. Under these settings, our algorithm converges after 12000 iterations.

SINR and achievable data rate: Figure 1 displays the cumulative distribution function (CDF) of (a) SINR and (b) achievable data rates, distinguishing between UAVs and gUEs. The results show an improvement of 3.7 dB in the 5%-tile SINR for UAVs, moving from -7.21 dB (Baseline) to -3.51 dB (Opt). Moreover, our solution offers a four-fold increase in the 5%-tile achievable data rate for UAVs, rising from 2 Mbps (Baseline) to 8 Mbps (Opt). Similar gains are observed in the mean SINR and mean achievable data rate. Furthermore, by varying only a single SSB beam from the baseline configuration while optimizing the network for UAVs, we incur a very limited gUEs performance degradation of 0.15 dB in the 5%-tile SINR and 1% in the the 5%-tile achievable data rate.

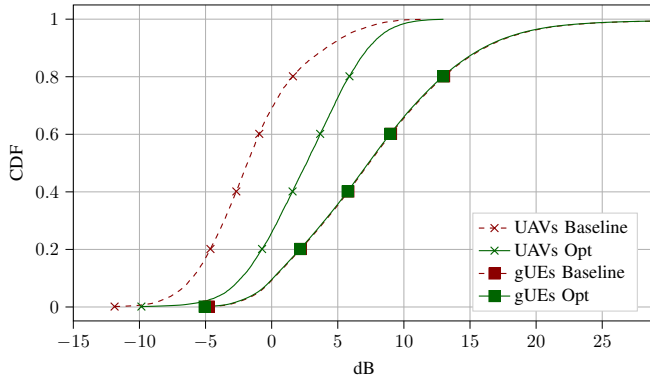
Traffic analysis: Figure 2 illustrates how the 5%-tile achievable data rate evolves as the traffic on the AH increases. For this analysis, we consider an increasing number of flying UAVs, up to 50, evenly spaced along the AH. When imposing a minimum data rate threshold of 5 Mbps, the baseline configuration can support only up to 5 UAVs. In contrast, our optimized solution can accommodate up to 15 UAVs, effectively tripling the traffic capacity on the AH.

V. CONCLUSION

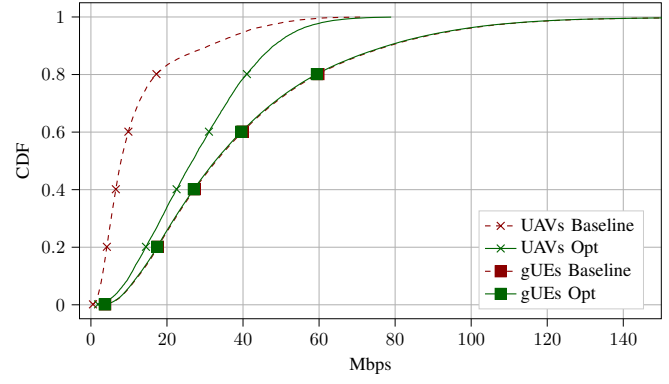
In this paper, we investigated how to provide optimal 5G connectivity from terrestrial mMIMO networks to UAVs within AHs, while minimizing impact on ground performance. We proposed a metric that optimally determines the serving cells for multiple segments of the AHs by jointly considering multiplexing capabilities, channel gains, and interference. Following this, we developed an algorithm to identify the optimal SSB beam planning strategy, thereby ensuring optimal coverage of the AHs from the selected cells. Simulation results demonstrated the benefits of our approach, with gains of up to four times in achievable data rates for UAVs. This illustrates that strategically and optimally controlling the selection of serving cells along the AH is crucial for enhancing UAVs capacity with minimal impact on ground performance. While in this paper we optimized the SSBs beams planning given a fixed AH partition, further performance gains may be achieved by optimizing the AH segmentation as well.

REFERENCES

- [1] Y. Zeng, I. Guvenc, R. Zhang, G. Geraci, and D. W. Matolak, *UAV Communications for 5G and Beyond*. John Wiley & Sons, 2020.
- [2] Q. Wu, J. Xu, Y. Zeng, D. W. K. Ng, N. Al-Dhahir, R. Schober, and A. L. Swindlehurst, “A comprehensive overview on 5G-and-beyond networks with UAVs: From communications to sensing and intelligence,” *IEEE J. Sel. Areas Commun.*, vol. 39, no. 10, pp. 2912–2945, 2021.
- [3] Y. Zeng, J. Lyu, and R. Zhang, “Cellular-connected UAV: Potential, challenges, and promising technologies,” *IEEE Wireless Commun.*, vol. 26, no. 1, pp. 120–127, Sep. 2019.
- [4] S. Kang, M. Mezzavilla, A. Lozano, G. Geraci, W. Xia, S. Rangan, V. Semkin, and G. Loianno, “Millimeter-wave UAV coverage in urban environments,” in *Proc. IEEE Globecom*, 2021.
- [5] Market Growth Reports, “Global Civil Drone Industry Research Report 2023, Competitive Landscape, Market Size, Regional Status and Prospect,” January 2023.
- [6] F.A.A., *Pilot’s Handbook of Aeronautical knowledge*. U.S. Department of Transportation, 2016.



(a) SINR Distribution



(b) Achievable Data Rate Distribution

Fig. 1. SINR and achievable data rate distribution for 12 UAVs on an AH positioned across cell edges at a height of 100 m.

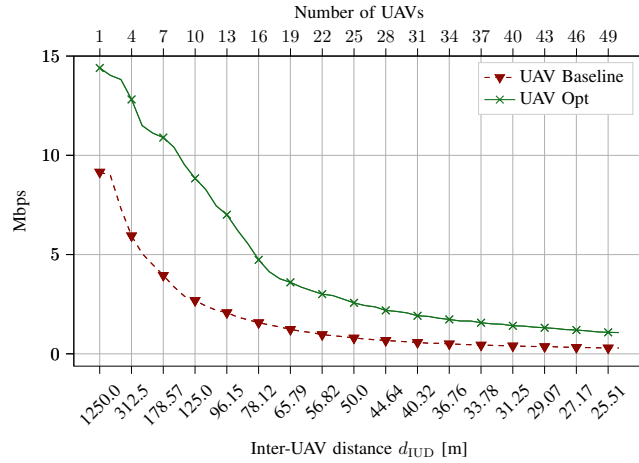


Fig. 2. 5%-tile achievable data rate for different traffic density and d_{IUD} .

- [7] N. Cherif, W. Jaafar, H. Yanikomeroglu, and A. Yongacoglu, "3D aerial highway: The key enabler of the retail industry transformation," *IEEE Commun. Mag.*, vol. 59, no. 9, pp. 65–71, Sep. 2021.
- [8] G. Geraci, A. Garcia-Rodriguez, M. M. Azari, A. Lozano, M. Mezzavilla, S. Chatzinotas, Y. Chen, S. Rangan, and M. D. Renzo, "What will the future of UAV cellular communications be? A flight from 5G to 6G," *IEEE Commun. Surveys Tuts.*, vol. 24, no. 3, pp. 1304–1335, 2022.
- [9] M. Mozaffari, X. Lin, and S. Hayes, "Toward 6G with connected sky: UAVs and beyond," *IEEE Commun. Mag.*, vol. 59, no. 12, pp. 74–80, 2021.
- [10] G. Geraci, D. López-Pérez, M. Benzaghta, and S. Chatzinotas, "Integrating terrestrial and non-terrestrial networks: 3D opportunities and challenges," *IEEE Commun. Mag.*, vol. 61, no. 4, pp. 42–48, 2023.
- [11] A. Colpaert, M. Raes, E. Vinogradov, and S. Pollin, "Drone delivery: Reliable cellular UAV communication using multi-operator diversity," in *Proc. IEEE Int. Conf. on Comm. (ICC)*, Aug. 2022, pp. 1–6.
- [12] H. Do, R. D. Pulgar, G. Fodor, and Z. Qi, "Cellular connectivity for advanced air mobility: Use cases and beamforming approaches," *IEEE Commun. Std. Mag.*, vol. 8, no. 1, pp. 65–71, 2024.
- [13] S. J. Maeng, M. M. U. Chowdhury, I. Güvenç, A. Bhuyan, and H. Dai, "Base station antenna up-tilt optimization for cellular-connected drone corridors," *IEEE Trans. Aerospace Elec. Systems*, vol. 59, no. 4, pp. 4729–4737, Jan. 2023.
- [14] M. M. U. Chowdhury, I. Güvenç, W. Saad, and A. Bhuyan, "Ensuring reliable connectivity to cellular-connected UAVs with up-tilted antennas and interference coordination," *ITU J. Fut. and Evol. Technol.*, pp. 165–185, Dec. 2021.
- [15] M. Bernabè, D. Lopez-Perez, D. Gesbert, and H. Bao, "On the optimization of cellular networks for UAV aerial corridor support," in *Proc. IEEE Global Commun. Conf. (GLOBECOM)*, Jan. 2022, pp. 2969–2974.

- [16] S. Karimi-Bidhendi, G. Geraci, and H. Jafarkhani, "Optimizing cellular networks for UAV corridors via quantization theory," *arXiv preprint arXiv:2308.01440*, 2023.
- [17] M. Benzaghta, G. Geraci, D. López-Pérez, and A. Valcarce, "Designing cellular networks for UAV corridors via Bayesian optimization," in *Proc. IEEE Global Commun. Conf. (GLOBECOM)*, Feb. 2023, pp. 4552–4557.
- [18] G. Geraci, A. Garcia-Rodriguez, L. Galati Giordano, D. López-Pérez, and E. Björnson, "Understanding UAV cellular communications: From existing networks to massive MIMO," *IEEE Access*, vol. 6, Nov. 2018.
- [19] A. Garcia-Rodriguez, G. Geraci, D. Lopez-Perez, L. G. Giordano, M. Ding, and E. Bjornson, "The essential guide to realizing 5G-connected UAVs with massive MIMO," *IEEE Commun. Mag.*, vol. 57, no. 12, pp. 84–90, Oct. 2019.
- [20] Y. Huang, Q. Wu, R. Lu, X. Peng, and R. Zhang, "Massive MIMO for cellular-connected UAV: Challenges and promising solutions," *IEEE Commun. Mag.*, vol. 59, no. 2, pp. 84–90, Feb. 2021.
- [21] D. Bethanabhotla, O. Y. Bursalioglu, H. C. Papadopoulos, and G. Caire, "Optimal user-cell association for massive MIMO wireless networks," *IEEE Trans. Wireless Commun.*, vol. 15, no. 3, pp. 1835–1850, Nov. 2016.
- [22] A. G. Gotsis, S. Stefanatos, and A. Alexiou, "Optimal user association for massive MIMO empowered ultra-dense wireless networks," in *Proc. IEEE Int. Conf. on Comm. Workshops (ICC Workshops)*, 2015, pp. 2238–2244.
- [23] M. Bernabè, D. López-Pérez, N. Piovesan, G. Geraci, and D. Gesbert, "Massive MIMO for aerial highways: Enhancing cell selection via SSB beams optimization," *IEEE O.J. on Commun.*, pp. 1–1, Jun. 2024.
- [24] 3GPP TR38.901, "Study on channel model for frequencies from 0.5 to 100 GHz," Mar. 2017, v.14.0.
- [25] 3GPP TR36.777, "Enhanced LTE support for aerial vehicles," Jan. 2017, v.15.0.
- [26] E. Björnson, J. Hoydis, and L. Sanguinetti, *Massive MIMO Networks: Spectral, Energy, and Hardware Efficiency*. Now Foundations and Trends, 2017.
- [27] 3GPP TR38.214, "Physical layer procedure for data," Sep. 2023, v.18.0.
- [28] E. Dahlman, S. Parkvall, and J. Skold, *5G NR: The Next Generation Wireless Access Technology*, 2nd ed. USA: Academic Press, Inc., 2018.
- [29] A. Giuliani, R. Nikbakht, G. Geraci, S. Kang, A. Lozano, and S. Rangan, "Spatially consistent air-to-ground channel modeling via generative neural networks," *IEEE Commun. Lett.*, vol. 13, no. 4, pp. 1158–1162, 2024.
- [30] A. P. Engelbrecht, *Computational intelligence: an introduction*. John Wiley & Sons, 2007.
- [31] J. H. Holland, "Genetic algorithms," *Scientific American*, vol. 267, no. 1, pp. 66–73, 1992.
- [32] D. Bhandari, C. Murthy, and S. K. Pal, "Genetic algorithm with elitist model and its convergence," *Internat. Journal of Pattern Recogn. and A.I.*, vol. 10, no. 06, pp. 731–747, 1996.
- [33] E. Vinogradov and S. Pollin, "Reducing safe UAV separation distances with U2U communication and new remote ID formats," in *Proc. IEEE Global Commun. Conf. Workshops (GLOBECOM Workshops)*, Jan. 2022, pp. 1425–1430.